coatings

Article

RETRACTED: Cathode Interlayer Engineering for Efficient Organic Solar Cells under Solar Illumination and Light-Emitting Diode Lamp

Iacopo Sîm Benesperi

Department of Chemistry, University of Surrey, Guildford GU2 7XH, UK; iacopo.benesperi28@gmail.com

Abstract: Organic solar cells (OSCs) have become a potential energy source for indoor light harvesting in recent years as they have witnessed a record power conversion efficiency (PCE) of over 30% under indoor lights. Among various strategies, interlayer engineering is one of the important factors in improving the performance of OSCs. Here, we reported an efficient OSC based on PM6:Y6 photoactive layer showing an excellent PCE of 22% and 14% under light-emitting diode (LED, 1000-lx) and 1-sun (AM1.5 G) conditions, respectively. The performance of OSCs was optimized by systematically investigating the optical, electrochemical, and morphological characteristics of three different cathode interlayers (CILs) named as: PEIE, ZnO, and ZnO/PEIE (bilayer). The high transmittance (~90%), suitable work function (~4.1 eV), and improved surface morphology (RMS: 2.61 nm) of the bilayer CIL contributes in improving the performance of OSCs. In addition, the suppressed charge recombination and improved charge carrier transport are attributed to high shunt resistance and appropriate energy levels alignment between photoactive layer and bilayer CIL. The findings in the study might provide guidelines for designing novel interlayers in the development of efficient OSCs for different illumination conditions.

Keywords: organic solar cells; photovoltaics; cathode interlayer; light-emitting diode lamp; power conversion efficiency

Citation: Benesperi, I.S. RETRACTED: Cathode Interlayer Engineering for Efficient Organic Solar Cells under Solar Illumination and Light-Emitting Diode Lamp. *Coatings* **2022**, *12*, 816. https://doi.org/10.3390/coatings12060816

Academic Editor: Alexander G. Ulyashin

Received: 21 May 2022
Accepted: 8 June 2022
Published: 10 June 2022
Retracted: 16 February 2023

1. Introduction

During the past decade, solution-processed organic solar cells (OSCs) have attracted immense attention for use in a promising renewable energy harvester due to numerous benefits such as cost-effectiveness, high stability, low weight, improved transparency, and scalable processing methods [1–8]. Besides, bandgap tuneability, high absorption coefficients, and availability of organic semiconductor materials in range of colors matches well with the spectral response of indoor light sources (light-emitting diode (LED), fluorescent (FL) lamps, etc.) that have a narrow emission spectrum spanning visible wavelengths (300–700 nm) and low intensity illumination (<1 mW/cm^2) [9–12]. Therefore, remarkable power conversion efficiency of over 31% has been achieved under indoor light conditions [13]. The high efficiencies of OSC are advantageous for powering small electronic devices that have been emerging in recent time [14–19].

The indoor light sources have different light intensities and spectrums than outdoor 1-sun illumination conditions as shown in Figure 1. Therefore, they require alternating strategies for performance improvement of OSCs. Strategies based on design of novel materials, interface, and electrode engineering and theoretical studies of OSC devices have been utilized [20–25]. In 2015, Mori et al. developed highly efficient OSCs with a reported power conversion efficiency of about 21% under LED lamp [26]. In 2020, Saeed et al. developed flexible OSCs based on P3HT:ICBA photoactive layer and achieved a PCE of over 10% under LED lamp [27]. They analyzed the influence of series and shunt resistance on the performance of OSCs. Similarly, CuI-doped P3HT:PCBM-based OSC have been

This paper has been retracted. A retraction notice was published on 16 February 2023 in *Coatings* **2023**, *13*, 446. https://doi.org/10.3390/coatings13020446

developed with a PCE of ~5% under white LED lamp [28]. The improved performance was attributed to the better hole selecting behavior and decreased charge carrier recombination.

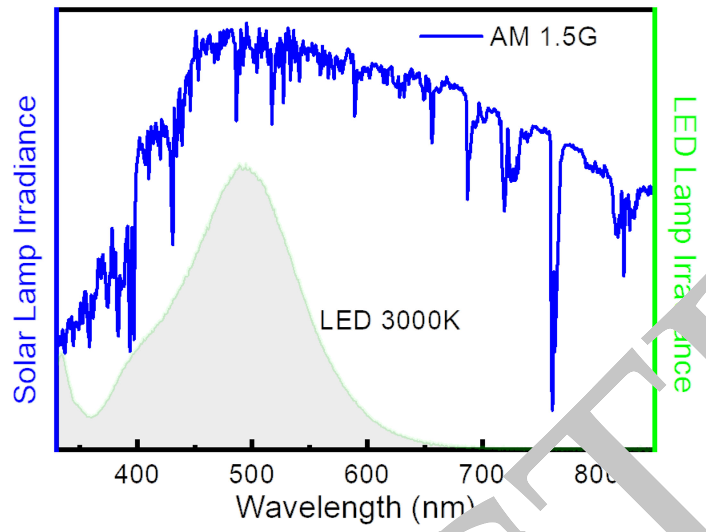

Figure 1. The spectral irradiance of the outdoor (1-sun) and indoor (LED 3000 K) light sources.

Under low-intensity light conditions, interlayer engineering is one of the crucial factors for developing high-performance OSCs. Unlike outdoor illumination where the series resistance plays a critical role, it is necessary to develop interlayers with high shunt resistance whereas the impact of series resistance become negligible under indoor light conditions [29,30]. Moreover, suitable work function alignment of interlayer with the photoactive layer is indispensable for achieving high-efficiency of OSCs. The low work function of electron-collecting electrode facilitates in reducing the charge recombination, thus leading to enhanced performance of OSCs. Previously ZnO, TiO_2, SnO_2, and PEIE interlayers have been used in OSCs [31–35]. However, until now, the role of interlayers in enhancing the performance of OSCs under indoor light conditions has not been fully understood and there is plenty of room available for further improvement.

In this study, we successfully developed high-performance OSCs based on a blend of Poly[[4,8-bis[5-(2-ethylhexyl)-4-fluoro-2-thienyl]benzo[1,2-b:4,5-b′]dithiophene-2,6-diyl]-2,5-thiophenediyl[5,7-bis(2-ethylhexyl)-4,8-dioxo-4H,8H-benzo[1,2-c:4,5 c′]dithiophene-1,3-diyl]-2,5-thiophenediyl]) (PM6) and (2,2′-((2Z,2′Z)-((12,13-bis(2-ethylhexyl)-3,9-diundecyl-12,13-dihydro-[1,2,5]thiadiazolo[3,4-e]thieno[2″,3″:4′,5′] thieno [2′,3′:4,5]pyrrolo[3,2-g]thieno thieno[2,3-b]indole-2,10-diyl)bis(methanylylidene)) bis(5,6-difluoro-3-oxo-2,3-dihydro-1H-indene-2,1-diylidene))dimalononitrile) (Y6) photoactive layer and investigated the performance evolution with three different types of cathode interlayers (CILs) (PEIE, ZnO, and PEIE/ZnO). ZnO and PEIE proved as excellent cathode interlayers due to high electron mobility, low toxicity, appropriate work function, and excellent transparency. We studied the optical, electrochemical, and morphological properties of CILs. Lastly, the OSCs with these types of CILs were fabricated in inverted geometry and achieved PCEs of around 15% and 18% under 1-sun and LED lamp illumination, respectively.

2. Materials and Methods

2.1. Materials

Zinc acetate dihydrate ($Zn(CH_3COO)_2.2H_2O$, 99%), 2-methoxyethanol ($CH_3OCH_2CH_2OH$, 99.8%), ethanolamine ($NH_2CH_2CH_2OH$, 99.5%), ethanol (C_2H_5OH, 99.8%), chloroform ($CHCl_3$, 99.6%), PEIE, and molybdenum(VI) oxide (MoO_3, 99.4%) were obtained from Sigma Aldrich, St. Louis, MO, USA. The donor PM6 and acceptor Y6 were purchased from Solarmer Material Inc., Beijing, China.

2.2. Device Fabrication

The pre-patterned ITO-coated glass (Sheet resistance: 12 Ω/sq. and transmittance: 95%) was washed inside an ultrasonic bath using deionized water (DI), acetone, and isopropyl alcohol (IPA) sequentially for 30 min each and then dried for 12 h in an oven. Prior to use, the substrates were UV-Ozone treated for 20 min to improve their work function. The ZnO solution was prepared by mixing 1.1 g of zinc acetate anhydrous and 0.30 g of ethanolamine with 10 mL of 2-methoxyethanol and then vigorously stirred overnight. PEIE was dissolved in 2-methoxyethanol to obtain a concentration of 0.3% and stirred overnight. The photoactive layer solution (1:1.2) was prepared as per a previous report [36]. CILs layers were deposited with a variable spin speed to achieve a thickness of 90–100 nm. Thermal annealing conditions for PEIE and ZnO were 120 °C for 10 min, and 180 °C for 30 min, respectively. The photoactive layer was deposited under nitrogen environment with a spin speed of 3000 rpm for 30 s followed by thermal annealing of 90 °C for 10 min. Finally, MoOx (10 nm) as anode interlayer and Ag (100 nm) as top electrode were subsequentially deposited using a thermal evaporator at a high vacuum pressure of 8.4×10^{-7} Pa.

2.3. Device Performance Characterization

The current density voltage (J-V) curves of all OSC devices were examined by Keithley 2400 m (Keithley Instruments, Cleveland, OH, USA) under nitrogen environment. For 1-sun, the J_{SC} was measured under AM1.5 G (100 mW/cm^2) using a Newport (North Kingstown, RI, USA) solar simulator. For indoor measurements, J-V curves were examined using a 1000 lux 3000 K LED (0.2 mW/cm^2) at room temperature under dark. IPCE measurement was conducted with Enlitech QE-R EQE (Kaohsiung City, Taiwan) system. The EQE system was equipped with standard silicon diode. The WF values of CILs were measured by Kelvin Probe (KP-TEK, Bullville, NY, USA). The transmittance spectra of CIL films were obtained by UV-visible spectroscopy (V-770, Jasco Inc., Easton, MD, USA). The film morphology of CIL films was measured by AFM instruments (Innova, BRUKER, Billerica, MA, USA).

3. Results and Discussion

The OSC devices with the inverted structure of ITO/CILs/PM6:Y6/MoOx/Ag are shown in Figure 2A. The chemical structure of photoactive layer material and energy band diagram of the OSC device are depicted in Figure 2B,C [33,37]. The inverted structure was employed to improve the stability of the devices.

The transmittance spectra of CILs of PEIE, ZnO, and ZnO/PEIE were measured by UV-vis spectroscopy and are shown in Figure 3. All the CILs showed an excellent averaged transmittance of over 90% in the visible region that suits well with the emission of LED lamp. The CIL_PEIE showed slightly high transmittance in the visible region while a decline of 5%–10% in the transmittance of CIL_ZnO and CIL_Bilayer between 400 to 550 nm was observed. It was anticipated that this slight reduction in the spectra will not have a significant effect on the photovoltaic performance of OSCs.

The morphological evolution in the surface of CILs on glass/ITO substrates was examined by AFM and shown in Figure 4. The root-mean-square (RMS) values of the ITO, CIL_PEIE, CIL_ZnO, and CIL_Bilayer were found to be 1.54 nm, 3.23 nm, 2.84 nm, and 2.61 nm, respectively. The RMS values of the CIL_PEIE and CIL_ZnO were slightly higher than that of the CIL_Bilayer with a smoother surface. This is because the uniform and smooth surfaces of CILs facilitate in improving the performance of OSCs due to low structural defects and enhanced charge collection efficiency [38]. Therefore, high performance for the CIL_Bilayer employed OSCs was expected.

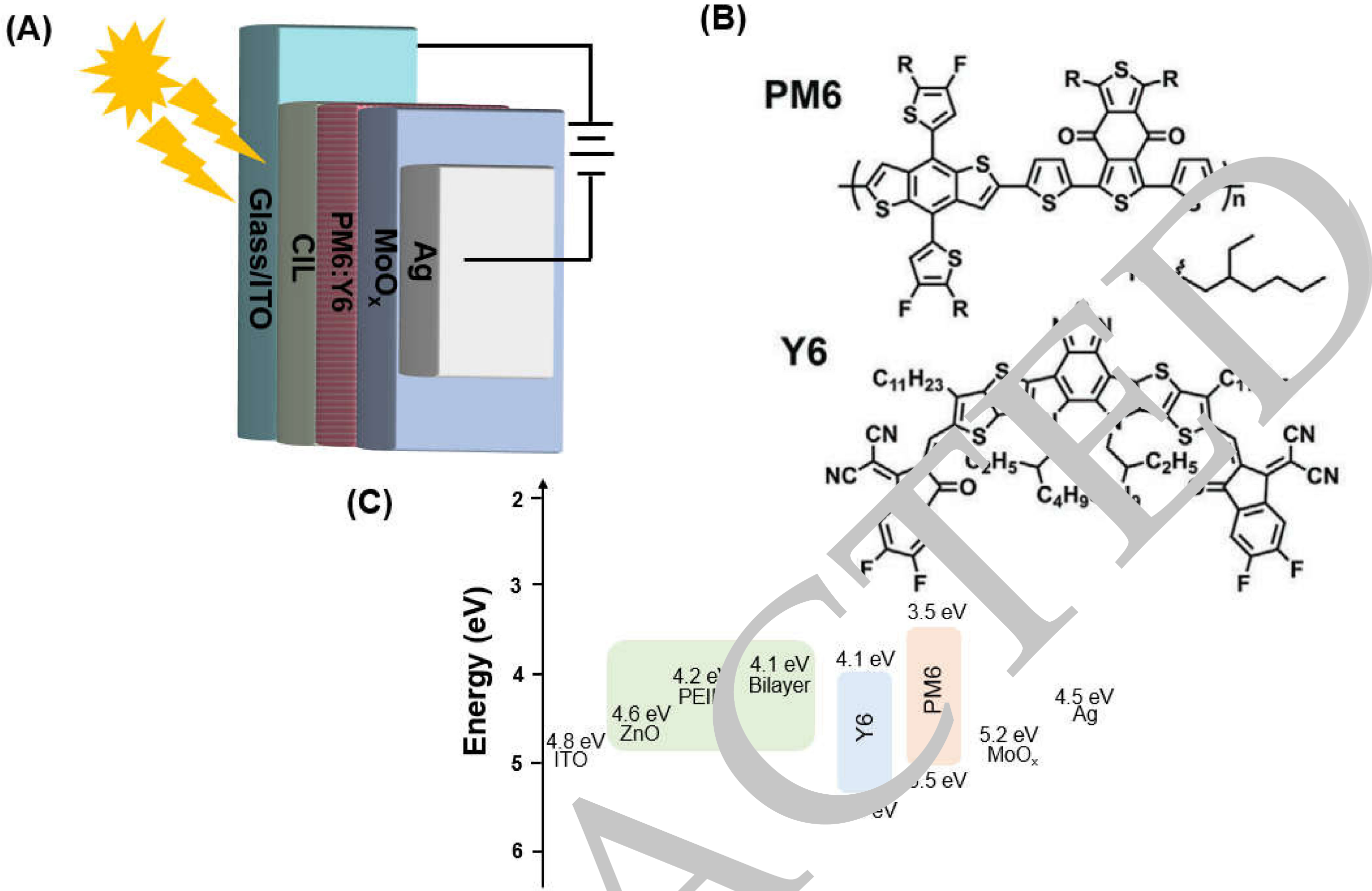

Figure 2. (**A**) The architecture of inverted OSC. (**B**) The chemical structures of photoactive layer materials (PM6 and Y6). (**C**) The energy level diagram of OSC.

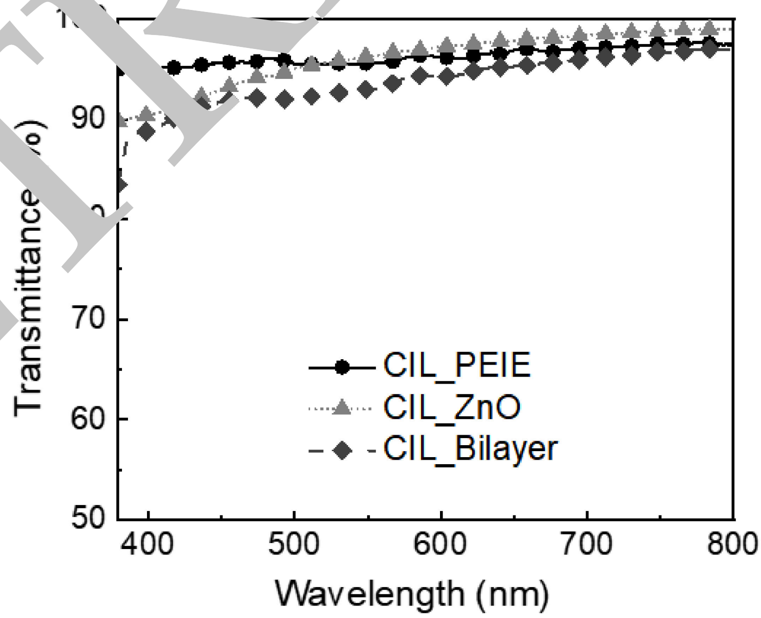

Figure 3. Transmittance spectra of various CILs investigated in this work.

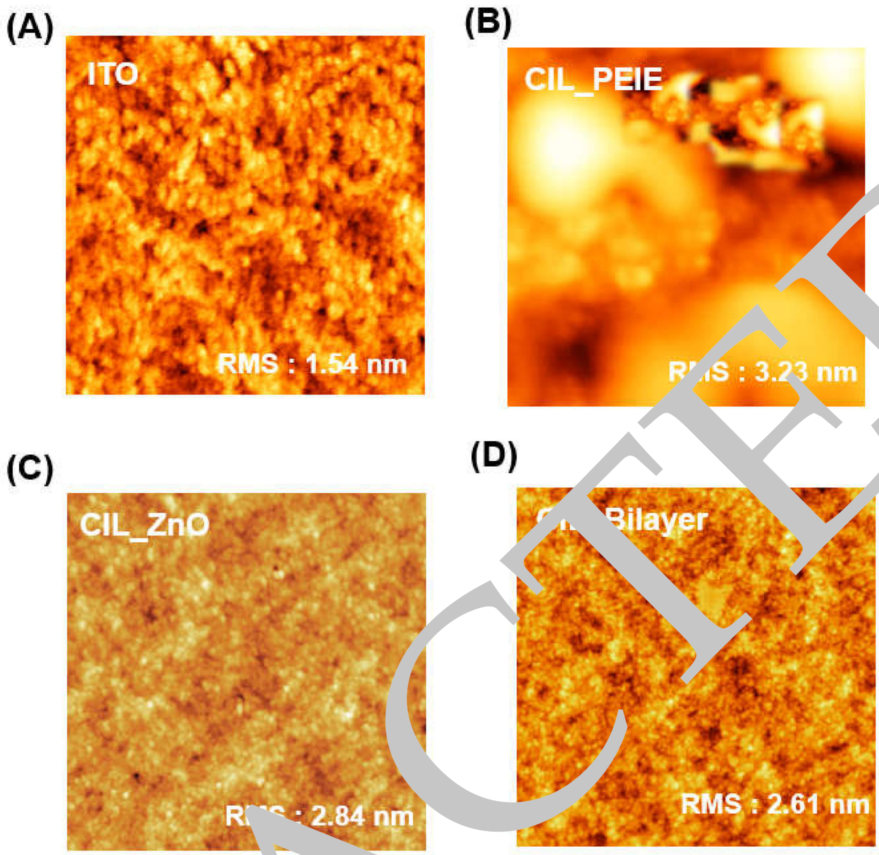

Figure 4. RMS roughness values of (**A**) ITO, (**B**) CIL-PEIE, (**C**) CIL_ZnO, and (**D**) CIL_Bilayer. (AFM Scan rate: 5 µm).

After validating the thin film properties of CILs, the photovoltaic performance of OSCs was examined under 1-sun illumination. The current-density voltage (J-V) curves of OSCs with different CILs was shown in Figure 5A. The measured J-V values can be determined [39,40] using Equation (1).

$$J = \left[J_o \left\{ \exp\left(\frac{q(V - JR_S)}{nKT} \right) - 1 \right\} + \left(\frac{V - JR_S}{R_{SH}} \right) \right] \quad (1)$$

where J_0 denotes the saturation reverse current density, n is the ideality factor, V is the output voltage, T is the temperature, q is the elementary charge, and R_S and R_{SH} are the series and shunt resistances, respectively.

The OSCs with CIL_PEIE exhibited a maximum PCE value of 12.1%, open-circuit voltage (V_{OC}) of 801 mV, short-circuit current density (J_{SC}) of 22.5 mA/cm^2, and fill factor (FF) of 66.8%. Similarly, the OSCs with CIL ZnO exhibited a PCE of 12.9% with a V_{OC} of 807 mV, J_{SC} of 23.6 mA/cm^2, and FF of 68.6. While, the improvement in the performance of OSC with CIL Bilayer was observed with a V_{OC} of 820 mV, a J_{SC} of 24.5 mA/cm^2, and FF of 69.0%, leading to the excellent PCE of 13.9%. The WF trend could be attributed to differences between the mechanism of WF reduction for PEIE surface modification, ZnO, and bilayer CILs. PEIE surface modification is known to induce a dipole moment on the conductor surface, leading to a vacuum-level downshift and resultantly WF reduction, while ZnO CIL leads to a semiconducting low-WF layer on top of the conductor surface. Further, the improved performance of the OSCs with CIL_Bilayer can be attributed to the enhanced oxygen desorption effect of ZnO when combined with the aminoacidic modified polymer PEIE [41]. The doping of PEIE with the ZnO improved the charge selectivity that led to enhancing the performance of OSCs. Further, the IPCE measurement was carried out to examine the discrepancies in the measured J_{SC} values (Figure 5B). The OSC devices with CIL_Bilayer showed a relatively high IPCE value of around 70% between 550 and 650 nm wavelength regions. While, the low IPCE value of CIL_PEIE was consistent with that of the measured J_{SC}. There was no significant difference observed before 450 nm and after 700 nm. The integrated J_{SC} values were found to be in agreement with the measured J_{SC} values. The summary of photovoltaic parameters (averaged over 10 OSC devices) was given in Table 1.

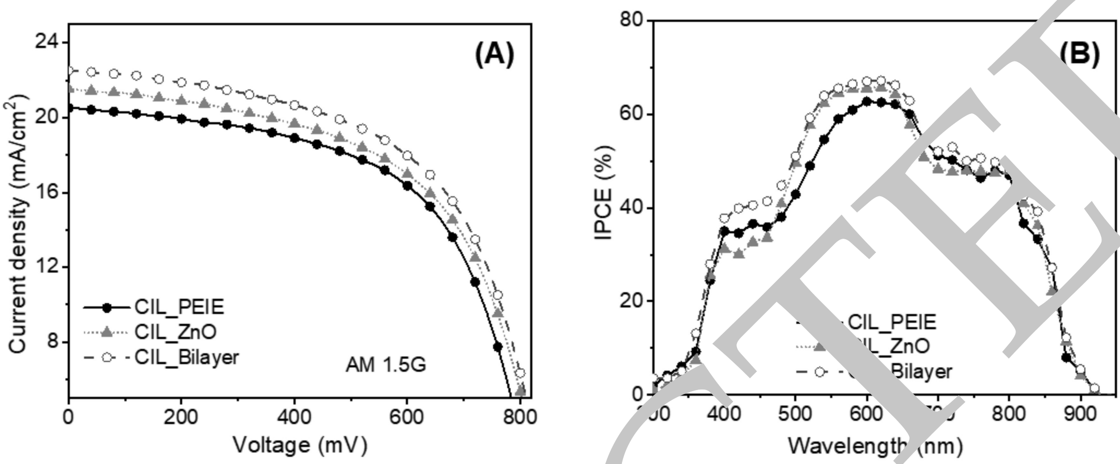

Figure 5. (**A**) The J-V curves and (**B**) IPCE spectra of OSCs with various CILs under 1-sun illumination condition.

Table 1. Summary of electrical parameters of OSCs under 1-sun conditions. Values are averaged over 10 devices. The values in brackets are amongst the highest.

CILs	V_{OC} (mV)	J_{SC} (mA/cm^2)	FF (%)	PCE (%)
CIL_PEIE	([illegible]) 798 ± [illegible]	(22.5) 21.5 ± 0.5	(66.8) 66.1 ± 1.0	(12.1) 11.6 ± 0.2
CIL_ZnO	(807) [illegible] ± 1	(23.6) 22.7 ± 0.5	(68.6) 68.1 ± 0.4	(12.9) 12.8 ± 0.1
CIL_Bilayer	(820) 817 ± 2	(24.5) 23.8 ± 0.3	(69.0) 68.9 ± 0.3	(13.9) 13.7 ± 0.1

As mentioned earlier, indoor lamps have totally different intensities and spectrum conditions when compared with the 1-sun conditions. Therefore, the evolution in the performance of OSCs under LED lamp was also systematically investigated. The J-V curves under 1000-lx LED 3000 K lamp was shown in Figure 6. The photovoltaic performance of the OSCs with CIL_Bilayer was recorded the highest with the maximum PCE value of 22.1%, a V_{OC} of 623 mV, a J_{SC} of 108.9 μA/cm^2, and FF of 71.6%. On the other hand, the OSCs with CIL_PEIE and CIL_ZnO exhibited maximum PCE values of 18.5% and 19.9%, with corresponding V_{OC} of 605 and 615 mV, J_{SC} of 100.4 and 102.9 μA/cm^2, and FF of 67.5% and 69.2%, respectively. There was a significant improvement in the J_{SC} value of CIL_Bilayer OSC observed that can be attributed to the improved absorption of photoactive layer.

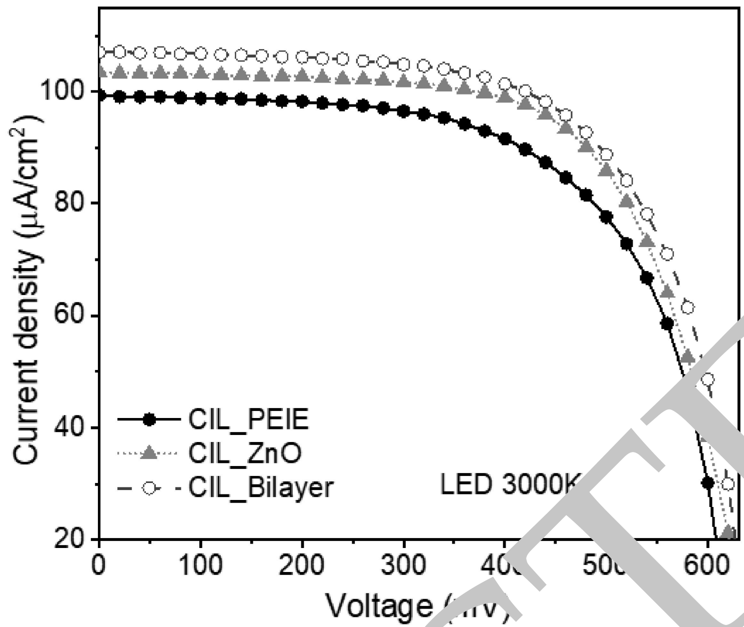

Figure 6. The J-V curves of OSC devices under 1000-lx LED 3000 K illumination.

In addition, the indoor performance of OSCs was further explained in the context of equivalent circuit model [42]. From that, V_{OC} depends on the light intensity logarithmically whereas the J_{SC} has a linear relation with the light intensity. Typically, the series resistance (R_S) has a strong impact (inverse relation) on the FF of OSCs under 1-sun illumination. However, under indoor conditions, this trend becomes reversed. Under LED lamps, instead of high R_S, it is important to obtain high shunt resistance (R_{sh}) that is associated with the leakage (dark) current. The high value of R_{sh} contributes in enhancing the FF of OSCs. As mentioned by previous reports, a minimum of 85 kΩ/cm^2 or larger values of R_{sh} and 50 Ω/cm^2 or smaller values of R_S are beneficial to obtain high performance under indoor lights. In our case, the R_{sh} and R_S values were calculated from the slopes of J-V characteristics curves. The extremely large R_{sh} values of the OSC devices (CIL_Bilayer > CIL_ZnO > CIL_PEIE) were found suitable to operate under indoor illumination conditions, consistent with the previous reports [43–45]. The summary of photovoltaic parameters along with resistance values is given in Table 2.

Table 2. Summary of electrical parameters of OSCs under 1000-lx LED 3000 K illumination. Values are averaged over 20 devices. The values in brackets are amongst the highest.

CILs	V_{OC} (mV)	J_{SC} (mA/cm^2)	FF (%)	PCE (%)	R_S (Ωcm^2)	R_{sh} (kΩcm^2)
CIL_PEIE	(605) 603 ± 2	(100.4) 99.5 ± 1.3	(67.5) 66.9 ± 0.9	(18.5) 17.9 ± 0.3	5.6	120
CIL_ZnO	(615) 611 ± 2	(103.3) 102.9 ± 0.9	(69.2) 68.7 ± 0.2	(19.9) 18.5 ± 0.2	4.3	132
CIL_Bilayer	(623) 618 ± 3	(108.9) 108.1 ± 0.4	(71.6) 70.4 ± 0.4	(22.1) 21.5 ± 0.2	2.4	144

Furthermore, the charge carrier recombination within the OSCs was determined by plotting the J_{SC} and V_{OC} as a function of light intensity (Figure 7). In Figure 7A, the J_{SC} was found to be linearly proportional to light intensity according to the (J_{SC} α slope (s) of light intensity) [46]. The value of s close to unity represents the minimum recombination. The fitted sloped values of the CILs were 0.91, 0.93, and 0.94 for the CIL_PEIE, CIL_ZnO, and CIL_Bilayer, respectively. The relatively high s value of the CIL_Bilayer suggests the suppression of charge carrier recombination.

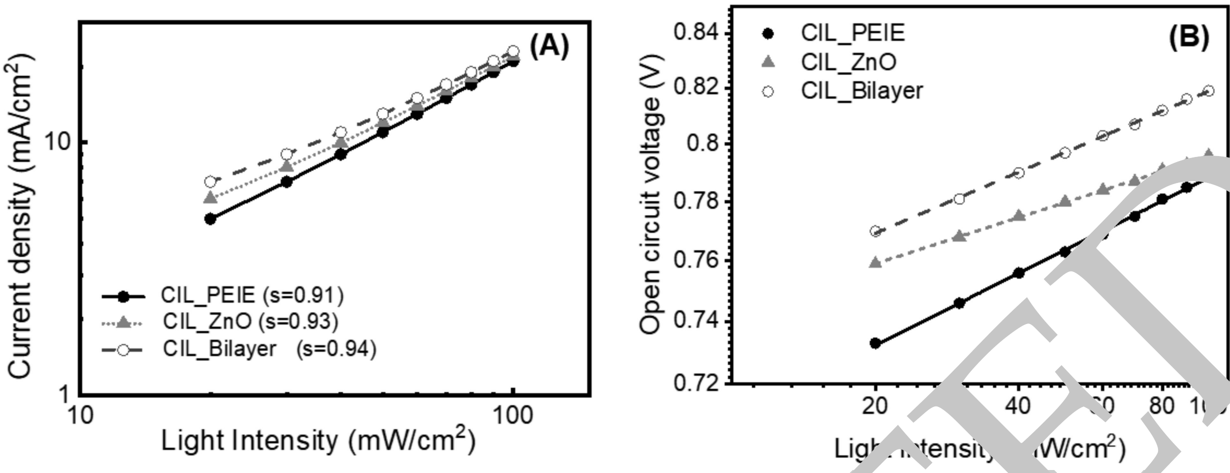

Figure 7. (**A**) The J_{SC} curves of OSC devices versus light intensity. (**B**) The V_{OC} curves of OSC devices versus light intensity.

Afterwards, V_{OC} is also crucial for gaining deep understanding the recombination kinetics. Figure 7B describes the logarithmic dependence of V_{OC} over light intensity. Mathematically, it can be expressed as,

$$V_{OC} = \frac{nkT}{q} \ln\left\{\frac{J_{ph}}{J_0}\right\} \quad (2)$$

where n is the ideality factor, k is the Boltzmann constant, T is the temperature, J_{ph} is the photocurrent density under illumination, while J_0 is the saturation current density under dark. n is the important factor that influences the proportionality between V_{OC} and light intensity. The values of n can be extracted by fitting the slope of curves. The extracted values of n for the CIL_PEIE, CIL_ZnO, and CIL_Bilayer were 1.42, 1.29, and 1.16, respectively. The value of n close to unity represents ideal diode behavior with zero loss, while that close to 2 describes the maximum charge recombination. From this analysis, it was obvious that OSCs with CIL_Bilayer exhibited the minimum recombination losses.

4. Conclusions

In conclusion, we examined the photovoltaic performance of OSCs based on various CILs under outdoor and indoor lighting conditions. There was a clear difference in the performance of OSC devices under both lighting conditions. The role of obtaining high R_{sh} is crucial under indoor lights while R_S influences the FF of the devices under 1-sun illumination. The optimized OSCs based on Bilayer_CIL exhibited the highest performance with the maximum PCE of 13.9% and 22.1% under AM1.5 G solar simulation and 1000-lx LED 3000 K illumination, respectively. The improvement in the surface morphology, transmittance, and external quantum efficiency resulted in the excellent performance of OSCs. In addition, the excellent performance of Bilayer-CIL-based OSCs can be attributed to the suitable work function and significant suppression in charge recombination. The results in the study set a foundation for realizing different types of CILs for the development of efficient OSC under outdoor and indoor light energy conditions.

Funding: This research received no external funding.

Institutional Review Board Statement: Not applicable.

Informed Consent Statement: Not applicable.

Data Availability Statement: Not applicable.

Conflicts of Interest: The authors declare no conflict of interest.

References

1. Lee, H.K.H.; Wu, J.; Barbé, J.; Jain, S.M.; Wood, S.; Speller, E.M.; Li, Z.; Castro, F.A.; Durrant, J.R.; Tsoi, W.C. Organic photovoltaic cells-promising indoor light harvesters for self-sustainable electronics. *J. Mater. Chem. A* **2018**, *6*, 5618–5626. [CrossRef]
2. Sun, Y.; Chang, M.; Meng, L.; Wan, X.; Gao, H.; Zhang, Y.; Zhao, K.; Sun, Z.; Li, C.; Liu, S.; et al. Flexible organic photovoltaics based on water-processed silver nanowire electrodes. *Nat. Electron.* **2019**, *2*, 513–520. [CrossRef]
3. Doumon, N.Y.; Dryzhov, M.V.; Houard, F.V.; Le Corre, V.M.; Chatri, A.R.; Christodoulis, P.; Koster, L.J.A. Photostability of Fullerene and Non-Fullerene Polymer Solar Cells: The Role of the Acceptor. *ACS Appl. Mater. Interfaces* **2019**, *11*, 8310–8318. [CrossRef] [PubMed]
4. Piva, N.; Greco, F.; Garbugli, M.; Iacchetti, A.; Mattoli, V.; Caironi, M. Tattoo-like transferable hole selective electrodes for highly efficient, solution-processed organic indoor photovoltaics. *Adv. Electron. Mater.* **2018**, *4*, 1700325. [CrossRef]
5. Saeed, M.A.; Yoo, K.; Cheol, H.C.; Shim, J.W.; Lee, J. Recent developments in dye-sensitized photovoltaic cells under ambient illumination. *Dyes Pigments* **2021**, *194*, 109626. [CrossRef]
6. Zhong, J.; Xiao, Z.; Liang, W.; Wu, Y.; Ye, Q.; Xu, H.; Deng, H.; Shen, L.; Feng, X.; Long, Y. Highly Efficient and High Peak Transmittance Colorful Semitransparent Organic Solar Cells with Hybrid-Electrode-Mirror Microcavity Structure. *ACS Appl. Mater. Interfaces* **2019**, *11*, 47992–48001. [CrossRef]
7. Saeed, M.A.; Shahzad, A.; Rasool, K.; Mateen, F.; Oh, J.M.; Shim, J.W. 2D MXene: A Potential Candidate for Photovoltaic Cells? A Critical Review. *Adv. Sci.* **2022**, *9*, 2104743. [CrossRef]
8. Ahmad, T.; Rahim, A.A.; Bilal, R.M.H.; Noor, A.; Maab, H.; Naveed, M.A.; Madni, [illegible]; Ali, M.M.; Saeed, M.A. Ultrawideband Cross-Polarization Converter Using Anisotropic Reflective Metasurface. *Electronics* **2022**, *11*, 487. [CrossRef]
9. You, Y.; Saeed, M.A.; Shafian, S.; Kim, J.; Kim, S.H.; Kim, S.H.; Kim, K.; Shim, J.W. Energy recycling under ambient illumination for internet-of-things using metal/oxide/metal-based colourful organic photovoltaics. *Nanotechnology* **2021**, *32*, 465401. [CrossRef]
10. Lee, T.; Oh, S.; Rasool, S.; Song, C.E.; Kim, D.; Lee, S.K.; Shin, W.S.; Lim, E. Non-halogenated solvent-processed ternary-blend solar cells: Via alkyl-side-chain engineering of a non-fullerene acceptor and their application in large-area devices. *J. Mater. Chem. A* **2020**, *8*, 10318–10330. [CrossRef]
11. Mateen, F.; Li, Y.; Saeed, M.A.; Sun, Y.; Zhang, Y.; Lee, S.Y.; Hong, S.K. Large-area luminescent solar concentrator utilizing donor-acceptor luminophore with nearly zero reabsorption: Indoor/outdoor performance evaluation. *J. Lumin.* **2021**, *231*, 117837. [CrossRef]
12. Park, S.Y.; Li, Y.; Kim, J.; Lee, T.H.; Walker, B.; Woo, H.Y.; [illegible] J.Y. Alkoxybenzothiadiazole-Based Fullerene and Nonfullerene Polymer Solar Cells with High Shunt Resistance for Indoor Photovoltaic Applications. *ACS Appl. Mater. Interfaces* **2018**, *10*, 3885–3894. [CrossRef] [PubMed]
13. Ma, L.K.; Chen, Y.; Chow, P.C.Y.; Zhang, G.; Huang, J.; Ma, C.; Zhang, J.; Yin, H.; Cheung, A.M.H.; Wong, K.S.; et al. High-efficiency indoor organic photovoltaics with a band-aligned interlayer. *Joule* **2020**, *4*, 1486–1500. [CrossRef]
14. Kim, S.; Jahandar, M.; Jeong, J.H.; Lim, D.C. Recent progress in solar cell technology for low-light indoor applications. *Curr. Altern. Energy* **2019**, *3*, 3–17. [CrossRef]
15. Du, N.; Schmidt, H.; Polian, I. Low-power emerging memristive designs towards secure hardware systems for applications in internet of things. *Nano Mater. Sci.* **2021**, *3*, 186–204. [CrossRef]
16. Michaels, H.; Rinderle, M.; Freitag, R.; Benesperi, I.; Edvinsson, T.; Socher, R.; Gagliardi, A.; Freitag, M. Dye-sensitized solar cells under ambient light powering machine learning: Towards autonomous smart sensors for the internet of things. *Chem. Sci.* **2020**, *11*, 2895–2906. [CrossRef]
17. Saeed, M.A.; Kang, H.C.; Yoo, K.; Asiam, F.K.; Lee, J.-J.; Shim, J.W. Cosensitization of metal-based dyes for high-performance dye-sensitized photovoltaics under ambient lighting conditions. *Dyes Pigments* **2021**, *194*, 109624. [CrossRef]
18. Kim, T.[illegible]; Lee, H.[illegible]; Saeed, M.A.; Son, J.H.; Woo, H.Y.; Kim, T.G.; Shim, J.W. Elastomeric Indoor Organic Photovoltaics with Superb Photothermal Endurance. *Adv. Funct. Mater.* **2022**, 2201921. [CrossRef]
19. Kim, S.H.; [illegible], C.H.; Saeed, M.A.; Ko, D.H.; Lee, J.H.; Shim, J.W. B-Cyclodextrin–Polyacryloyl Hydrazide-Based Surface Modification for Efficient Electron-Collecting Electrodes of Indoor Organic Photovoltaics. *J. Mater. Res. Technol.* **2022**, *16*, 165[illegible]–1666. [CrossRef]
20. Hashemi, S.A.; Ramakrishna, S.; Aberle, A.G. Recent progress in flexible-wearable solar cells for self-powered electronic devices. *Energy Environ. Sci.* **2020**, *13*, 685–743. [CrossRef]
21. Yin, H.; [illegible]; Cheung, S.H.; Li, H.W.; Xie, Y.; Tsang, S.W.; Zhu, X.; So, S.K. Porphyrin-based thick-film bulk-heterojunction solar cells for indoor light harvesting. *J. Mater. Chem. C* **2018**, *6*, 9111–9118. [CrossRef]
22. Kim, G.P.; Jeon, S.J.; Moon, D.K. Design Principles and Synergistic Effects of Chlorination on a Conjugated Backbone for Efficient Organic Photovoltaics: A Critical Review. *Adv. Mater.* **2020**, *32*, e1906175. [CrossRef] [PubMed]
23. Kim, S.; Saeed, M.A.; Kim, S.H.; Shim, J.W. Enhanced hole selecting behavior of WO3 interlayers for efficient indoor organic photovoltaics with high fill-factor. *Appl. Surf. Sci.* **2020**, *527*, 146840. [CrossRef]
24. Lechêne, B.P.; Cowell, M.; Pierre, A.; Evans, J.W.; Wright, P.K.; Arias, A.C. Organic solar cells and fully printed super-capacitors optimized for indoor light energy harvesting. *Nano Energy* **2016**, *26*, 631–640. [CrossRef]
25. Kim, S.H.; Saeed, M.A.; Lee, S.Y.; Shim, J.W. Investigating the indoor performance of planar heterojunction based organic photovoltaics. *IEEE J. Photovolt.* **2021**, *11*, 997–1003. [CrossRef]

26. Mori, S.; Gotanda, T.; Nakano, Y.; Saito, M.; Todori, K.; Hosoya, M. Investigation of the organic solar cell characteristics for indoor LED light applications. *Jpn. J. Appl. Phys.* **2015**, *54*, 071602. [CrossRef]
27. Saeed, M.A.; Kim, S.H.; Lee, S.Y.; Shim, J.W. High indoor performance of flexible organic photovoltaics using polymer electrodes. *Thin Solid Films* **2020**, *704*, 138006. [CrossRef]
28. Khairulaman, F.L.; Yap, C.C.; Jumali, M.H.H. Improved performance of inverted type organic solar cell using copper iodide-doped P3HT:PCBM as active layer for low light application. *Mater. Lett.* **2021**, *283*, 128827. [CrossRef]
29. Steim, R.; Ameri, T.; Schilinsky, P.; Waldauf, C.; Dennler, G.; Scharber, M.; Brabec, C.J. Organic photovoltaics for low light applications. *Sol. Energy Mater. Sol. Cells* **2011**, *95*, 3256–3261. [CrossRef]
30. Reich, N.H.; van Sark, W.G.J.H.M.; Alsema, E.A.; Lof, R.W.; Schropp, R.E.I.; Sinke, W.C.; Turkenburg, W.C. Crystalline silicon cell performance at low light intensities. *Sol. Energy Mater. Sol. Cells* **2009**, *93*, 1471–1481. [CrossRef]
31. Nam, M.; Baek, S.; Ko, D.H. Unraveling optimal interfacial conditions for highly efficient and reproducible organic photovoltaics under low light levels. *Appl. Surf. Sci.* **2020**, *526*, 146632. [CrossRef]
32. Lee, J.; You, Y.; Saeed, M.A.; Kim, S.H.; Choi, S.; Kim, S.; Lee, S.Y.; Park, J.; Shim, J.W. Undoped tin dioxide transparent electrodes for efficient and cost-effective indoor organic photovoltaics (SnO_2 electrode for indoor organic photovoltaics). *NPG Asia Mater.* **2021**, *13*, 43. [CrossRef]
33. Goo, J.S.; Shin, S.C.; You, Y.J.; Shim, J.W. Polymer surface modification to optimize inverted organic photovoltaic devices under indoor light conditions. *Sol. Energy Mater. Sol. Cells* **2018**, *184*, 31–37. [CrossRef]
34. Cao, Y.; Liu, Y.; Zakeeruddin, S.M.; Hagfeldt, A.; Grätzel, M. Direct contact of selective charge extraction layers enables high-efficiency molecular photovoltaics. *Joule* **2018**, *2*, 1108–1117. [CrossRef]
35. Sattar, A.; Farooq, M.; Amjad, M.; Saeed, M.A.; Nawaz, S.; Mujtaba, M.A.; Anwar, S.; El-Sherbeeny, A.M.; Soudagar, M.E.M.; Filho, E.P.B.; et al. Performance evaluation of a direct absorption collector for solar thermal energy conversion. *Energies* **2020**, *13*, 4956. [CrossRef]
36. Zhu, L.; Zhang, M.; Zhou, G.; Hao, T.; Xu, J.; Wang, J.; Qiu, C.; Prine, N.; Ali, J.; Feng, W.; et al. Efficient Organic Solar Cell with 16.88% Efficiency Enabled by Refined Acceptor Crystallization and Morphology with Improved Charge Transfer and Transport Properties. *Adv. Energy Mater.* **2020**, *10*, 1904234. [CrossRef]
37. Shin, S.C.; You, Y.J.; Goo, J.S.; Shim, J.W. In-depth interfacial engineering for efficient indoor organic photovoltaics. *Appl. Surf. Sci.* **2019**, *495*, 143556. [CrossRef]
38. Saeed, M.A.; Kim, S.H.; Kim, H.; Liang, J.; Woo, H.Y.; Lee, T.G.; Yan, H.; Shim, J.W. Indoor organic photovoltaics: Optimal cell design principles with synergistic parasitic resistance and optical modulation effect. *Adv. Energy Mater.* **2021**, *11*, 2003103. [CrossRef]
39. Kippelen, B.; Brédas, J.L. Organic photovoltaics. *Energy Environ. Sci.* **2009**, *2*, 251–261. [CrossRef]
40. Saeed, M.A.; Kim, S.H.; Baek, K.; Jerome, G.; Lee, S.Y.; Shim, J.W. PEDOT: PSS: CuNW-based Transparent Composite Electrodes for High-Performance and Flexible Organic Photovoltaics under indoor lighting. *Appl. Surf. Sci.* **2021**, *567*, 150852. [CrossRef]
41. Qin, F.; Wang, W.; Sun, L.; Jiang, X.; Hu, L.; Xiong, S.; Liu, T.; Dong, X.; Li, J.; Jiang, Y.; et al. Robust metal ion-chelated polymer interfacial layer for ultraflexible non-fullerene organic solar cells. *Nat. Commun.* **2020**, *11*, 4508. [CrossRef] [PubMed]
42. Qi, B.; Wang, J. Open-circuit voltage in organic solar cells. *J. Mater. Chem.* **2012**, *22*, 24315–24325. [CrossRef]
43. Saeed, M.A.; Cheng, S.; Biswas, S.; Hyeon, W.; Kwon, S.; Kim, H.; Kim, Y.; Shim, J.W. Remarkably high performance of organic photovoltaic devices with [illegible]9-bis dithiophen[illegible]thylhexyloxy] photoactive acceptor under halogen light illumination. *J. Power Sources* **2022**, *518*, 230782. [CrossRef]
44. Stubhan, T.; Li, N.; Luechinger, N.A.; Halim, S.C.; Matt, G.J.; Brabec, C.J. High fill factor polymer solar cells incorporating a low temperature solution processed WO_3 hole extraction layer. *Adv. Energy Mater.* **2012**, *2*, 1433–1438. [CrossRef]
45. Rafique, S.; Abdullah, S.M.; Shahid, M.M.; Ansari, M.O.; Sulaiman, K. Significantly improved photovoltaic performance in polymer bulk heterojunction solar cells with graphene oxide /PEDOT:PSS double decked hole transport layer. *Sci. Rep.* **2017**, *7*, 39555. [CrossRef]
46. Singh, R.; Duan, T.; Kan, Z.; Chochos, C.L.; Kini, G.P.; Kumar, M.; Park, J.; Lee, J.; Lee, J.J. Revealing the structural effects of non-fullerene acceptors on the performances of ternary organic photovoltaics under indoor light conditions. *Nano Energy* **2020**, *75*, 104934. [CrossRef]